

**ICSV14**  
Cairns • Australia  
9-12 July, 2007



## **OPTIMAL CONTROL OF A PRETWISTED TAPERED ROTATING BEAM WITH TIP ROTOR.**

Naresh K. Chandiramani<sup>1</sup> and Liviu Librescu<sup>2</sup>

<sup>1</sup>Department of Civil Engineering, Indian Institute of Technology Bombay  
Powai, Mumbai 400076, India

<sup>2</sup>Department of Engineering Science and Mechanics, Virginia Tech.  
Blacksburg, VA 24061-0219, USA

[naresh@civil.iitb.ac.in](mailto:naresh@civil.iitb.ac.in) (email address of lead author or presenter)

### **Dedication**

The first author would like to dedicate this paper to the memory of the second author. Professor Liviu Isidor Librescu died on April 16, 2007, while on duty. He was teaching class when the mass shootings occurred at the ESM department at Virginia Tech. Dr. Librescu was a very fine and caring person, outstanding academician, and an inspiring graduate research advisor. His heroic act during his last moments, which helped save the lives of students in his classroom, is well documented. His fond memories shall be cherished and will continue to inspire.

### **Abstract**

Active control of a thin-walled rotating beam with pretwist, double-taper, and a tip rotor, is considered using the higher-order shear deformation theory (HSDT). The beam comprises an orthotropic host with surface-embedded transversely isotropic (PZT-4) sensor-actuator pairs. Span-wise and thickness-wise variation is considered for the electric field applied to actuators. This yields a coupled electro-mechanical system, wherein displacement variables are coupled via the electric field. Optimal LQR control with state feedback is used to obtain the control input (charge density applied to actuators). Parametric studies involving ply-angle, rotation speeds of beam and rotor, pretwist, taper, rotor mass, and saturation constraint on actuator voltage, are performed. The present model yields an order-of-magnitude reduction in settling time and control voltage/power, and lower response, vis-a-vis the decoupled approach.

## **1. INTRODUCTION**

Fiber-reinforced composites with embedded piezoelectric elements provide a synthesis of passive and active control. Design of optimal controllers - yielding reduced settling time and control energy - require an accurate plant model incorporating shearability, satisfaction of traction free boundary conditions (BCs), warping restraint, etc.

Kim and White [1] analyzed a non-rotating thick-walled beam using a cubic variation of axial displacements to satisfy the traction free BCs. Eigenvibration analyses for rotating blades were done by Jung et. al. [2] within the First-Order Shear Deformation Theory (FSDT), by

Song et al. [3] for a beam with tip rotor, and by Chandiramani et al. [4] considering a pretwisted composite blade and the HSDT. Significant eigenfrequency enhancements were reported in the latter work, which was extended by Shete et al. [5] for optimal control using PZT actuation and an uncoupled electromechanical formulation. A pretwisted blade with a tip mass was analyzed by Yoo et al. [6] by retaining gyroscopic effects and using hybrid deformation variables to linearize the system.

Kunz [7] analyzed a saturation controller and found it effective in reducing tip responses even at moderately high rotation speeds and despite significant intermodal coupling. Cai and Lim [8] designed an optimal tracking controller for a flexible hub-beam system by neglecting the axial deformation effects. Wei et al. [9] presented experimental results on control of an angular-accelerating sandwich-beam comprising an ER fluid core with aluminium surface layers. Choi et al. [10] considered PVDF sensors and piezoelectric fibers for actuation (i.e., macro-fiber composites – MFC's) using negative velocity feedback control.

Optimal control of flexural vibration in a composite plate - with piezo sensors/actuators covering the plan - was studied by Ray [11] using output feedback and coupled charge-mechanical equations. Genetic algorithms for optimal sensor/actuator placement have been used by Han and Lee [12] using controllability, observability, and spillover prevention criteria, and by Liu et al. [13] using the  $H^2$  norm.

Herein, a HSDT model for pretwisted, composite blades [5] is extended to include a tip rotor, double-taper, and spanwise distributed PZT-4 sensor-actuator pairs. The coupled electromechanical system is solved using optimal control with state feedback, to obtain the control input. Influence of shear deformation, pretwist and taper, and the tip rotor are assessed.

## 2. FORMULATION

Consider a straight, pretwisted, doubly-tapered, single celled box beam with tip rotor (mass  $m_R$ , spin speed  $\Omega \mathbf{k}_R$ ) mounted on a rigid hub (radius  $R_0$ , rotation speed  $\Omega \mathbf{j} = \Omega \mathbf{j}$ ) (Fig. 1).

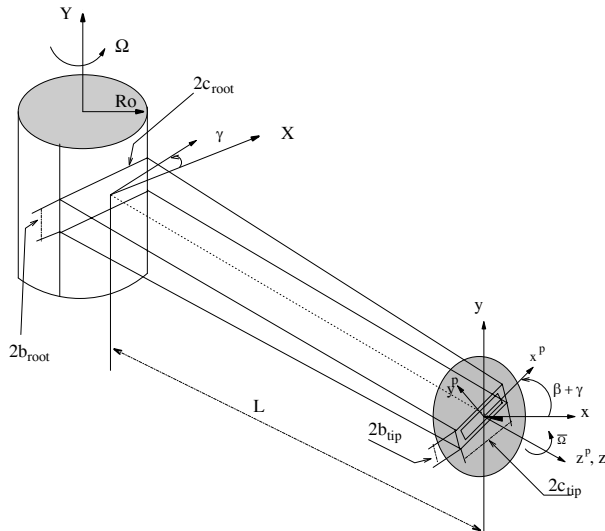


Figure 1. Tapered beam with tip rotor.

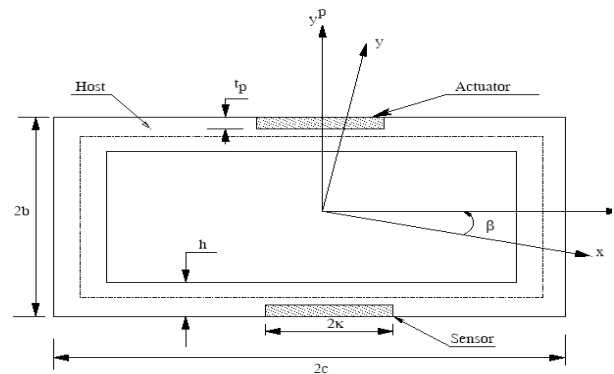


Figure 2. Cross-sectional view.

The beam-fixed coordinate system  $(x, y, z)$  originates at the beam root,  $(s, n, z)$  is a local (surface) coordinate system, and  $(x^p, y^p, z^p)$  are local coordinates along the cross section principal axes. The beam-fixed and rotor-fixed bases are  $(\mathbf{i}, \mathbf{j}, \mathbf{k})$  and  $(\mathbf{i}_R, \mathbf{j}_R, \mathbf{k}_R)$ , respectively. The coordinates are defined as

$$\bar{x}[s, z] = \bar{x}^p[s] \cos \beta - \bar{y}^p[s] \sin \beta; \quad \bar{y}[s, z] = \bar{x}^p[s] \sin \beta + \bar{y}^p[s] \cos \beta; \quad z = z^p \quad (1)$$

where the overbar denotes mid-surface quantities ( $n = 0$ ). The quadratically varying pretwist is considered as  $\beta[z] = \gamma + \beta_0 z/L + \beta_1 (z/L)^2$

## 2.1 Kinematics

The assumptions include a spanwise dependent twist rate, quadratic variation of transverse shear strains through wall thickness, secondary warping, and no in-plane cross-section distortion. Imposing the traction free BC's yields the transverse shear strain distribution (HSDT) as

$$\gamma_{xz} = (1 - 4n^2/h^2)\bar{\gamma}_{xz}[z;t]; \quad \gamma_{yz} = (1 - 4n^2/h^2)\bar{\gamma}_{yz}[z;t] \quad (2)$$

The lag ( $u[x, y, z;t]$ ), flap ( $v[x, y, z;t]$ ), and extensional ( $w[x, y, z;t]$ ) displacements are obtained in terms of the corresponding displacements  $u_o[z;t]$ ,  $v_o[z;t]$ ,  $w_o[z;t]$  of a reference point  $O[0,0]$  on the cross-section, twist  $\phi[z;t]$ , and the rotations  $\theta_x[z;t]$  and  $\theta_y[z;t]$  about  $x$  and  $y$  axes, respectively (Chandiramani et al. [4]).

## 2.2 Piezopatch Distribution

The PZT-4 sensor and actuator patches are embedded on the bottom and top face, respectively, with their surface of isotropy being parallel to the mid-surface of the pretwisted beam (Fig. 2). The electric potential distribution  $\psi[s, n, z;t] = n\psi_o[z;t]$  is considered, yielding the electric field as

$$E_1 = -\partial\psi/\partial s = 0; \quad E_2 = -\partial\psi/\partial z = -n\psi'_o; \quad E_3 = -\partial\psi/\partial n = -\psi_o[z;t] \quad (3)$$

## 2.3 Stress Field

The stress-strain relation for a constituent beam-wall layer is

$$\begin{Bmatrix} \sigma_{ss} \\ \sigma_{zz} \\ \sigma_{sz} \end{Bmatrix} = \begin{bmatrix} \bar{Q}_{11} & \bar{Q}_{12} & \bar{Q}_{16} \\ \bar{Q}_{12} & \bar{Q}_{22} & \bar{Q}_{26} \\ \bar{Q}_{16} & \bar{Q}_{26} & \bar{Q}_{66} \end{bmatrix} \begin{Bmatrix} \varepsilon_{ss} \\ \varepsilon_{zz} \\ \gamma_{sz} \end{Bmatrix} - \begin{Bmatrix} \bar{\zeta}_{31}E_3 \\ \bar{\zeta}_{31}E_3 \\ 0 \end{Bmatrix}; \quad \begin{Bmatrix} \tau_{nz} \\ \tau_{ns} \end{Bmatrix} = \begin{bmatrix} \bar{Q}_{44} & \bar{Q}_{45} \\ \bar{Q}_{45} & \bar{Q}_{55} \end{bmatrix} \begin{Bmatrix} \gamma_{nz} \\ \gamma_{ns} \end{Bmatrix} - \begin{Bmatrix} \bar{\zeta}_{15}E_2 \\ 0 \end{Bmatrix} \quad (4)$$

where,  $\bar{Q}_{ij}$  and  $\bar{\zeta}_{ij}$  are transformed reduced stiffnesses and reduced piezoelectric coefficients of the composite beam (details omitted for brevity). Introducing the strain field and integrating over the cross-section, these 3-D constitutive equations are reduced to a 1-D dependency, thus yielding the beam forces and moments.

## 2.4 Governing Equations of Motion

Hamiltons principle for the beam with rotor reads

$$\int_{t_0}^{t_1} \left[ \int_{\tau} (\delta\tilde{H} + \rho\ddot{\mathbf{R}} \cdot \delta\mathbf{R}) d\tau + \int_{\tau_R} (\rho_R \ddot{\mathbf{R}}_R \cdot \delta\mathbf{R}_R) d\tau_R - \int_{\zeta} (\bar{\sigma}_k \delta U_k - \bar{\sigma} \delta\psi) d\zeta \right] dt = 0 \quad (5)$$

where,

$$\begin{aligned} \tilde{H} &= 0.5[\sigma_{zz}\varepsilon_{zz} + \tau_{sz}\gamma_{sz} + \tau_{nz}\gamma_{nz}] - \zeta_{31}E_3\varepsilon_{zz} - 0.5[\xi_{11}E_1^2 + \xi_{22}E_2^2 + \xi_{33}E_3^2]; \\ \mathbf{R} &= [x + u]\mathbf{i} + [y + v]\mathbf{j} + [R_0 + z + w]\mathbf{k}; \\ \mathbf{R}_R &= u_o\mathbf{i} + v_o\mathbf{j} + (L + w_o + R_0)\mathbf{k} + x\mathbf{i}_R + y\mathbf{j}_R + (r_m + z)\mathbf{k}_R \end{aligned} \quad (6)$$

Here  $\bar{\sigma}_k$ ,  $U_k$ ,  $\bar{\sigma}$ ,  $\psi$ ,  $\tilde{H}$ ,  $\mathbf{R}$ ,  $\mathbf{R}_R$ , and  $\xi_{ij}$  denote surface traction vector, displacement vector, applied surface charge density, electric potential, electric enthalpy, position vector for deformed beam, position vector for rotor, and dielectric constants (details omitted), respectively.

A vertical (y-directed) line load,  $p_y[z;t]$  is assumed. The resulting seven electromechanical equations of motion (EOM) and BC's exhibit a 1-D dependency on the spanwise ( $z$ ) coordinate, and are in terms of displacement field variables  $u_o$ ,  $v_o$ ,  $\theta_x$ ,  $\theta_y$ ,  $w_o$ ,  $\phi$ , and electric potential  $\psi_o$ . Since the beam is directed radially outward from the hub, Coriolis effects due to beam rotation ( $\Omega$ ) are negligible. The Circumferentially Uniform Stiffness (CUS) ply angle configuration is considered (Song et al. [3]). This yields a linearized and coupled system governing the motion (bending - transverse shear, i.e., flap-lag, and extension-twist) and the electric potential. The coupling occurs via  $\psi_o$ . When a spatially constant electric potential is assumed, flap-lag and extension-twist motions decouple in contrast to the present case. Representative ( $u_o$  and  $\psi_o$ ) EOM's are:

$$\begin{aligned} \delta u_o : \{ & [\delta_h I_1 + \delta_e I_7](\ddot{u}'_o - \Omega^2 u'_o)\}' + \{ [\delta_h I_5 + \delta_e I_9](\ddot{v}'_o - \Omega^2 v'_o)\}' + \delta_h \{ [I_3 - I_1](\ddot{\theta}'_y - \Omega^2 \theta'_y)\}' - \\ & \delta_h \{ [I_6 - I_5](\ddot{\theta}'_x - \Omega^2 \theta'_x)\}' - b_1(\ddot{u}_o - \Omega^2 u_o) - \delta_e (a_{22}u''_o + a_{23}v''_o) + (b_1\Omega^2 R u'_o)' + \\ & \delta_t \{ (a_{44} + \delta_h \tilde{a}_1)(u'_o - \theta_y) + (a_{43} + \delta_h \tilde{a}_2)\theta'_x + (\delta_h \tilde{a}_{30} - a_{42})\theta'_y + (a_{45} + \delta_h \tilde{a}_{31})(v'_o + \theta_x)\}' + \quad (7) \\ & \delta_h \{ [\tilde{a}_3 v''_o + \tilde{a}_{32} u''_o]' + [\tilde{a}_5 \theta'_y - \tilde{a}_6 u''_o - \tilde{a}_4 (v'_o + \theta_x) - \tilde{a}_{34} \theta'_x - \tilde{a}_{35} v''_o - \tilde{a}_{32} (u'_o - \theta_y)]\}' + \\ & \delta_t (\tilde{a}_{P2} \psi_o - \tilde{a}_{P13} \psi'_o)' - \delta_e (\tilde{a}_{P9} \psi_o)'' - \delta_h (\tilde{a}_{P8} \psi_o)'' = 0 \end{aligned}$$

$$\begin{aligned} \delta \psi_o : & L_{P22} \psi''_o - L_{P33} \psi_o + \tilde{a}_{P1} w'_o + \tilde{a}_{P4} \theta'_x - \tilde{a}_{P5} \theta'_y - (\tilde{a}_{P7} - \tilde{a}_{P6}) v''_o - (\tilde{a}_{P9} + \tilde{a}_{P8}) u''_o + \tilde{a}_{P10} \phi' - \\ & \tilde{a}_{P2} u'_o - \tilde{a}_{P3} v'_o + \tilde{a}_{P4} \theta_x + \tilde{a}_{P2} \theta_y = a_{P10} \bar{\sigma} \quad (8) \end{aligned}$$

The boundary conditions at the clamped end ( $z = 0$ ) are

$$u_o = v_o = \theta_y = \theta_x = u'_o = v'_o = w_o = \phi = \phi' = \psi_o = 0 \quad (9)$$

Here ( $\tilde{a}_{ij}[z]$ ,  $a_{ij}[z]$ ) are global stiffnesses, the former including pretwist and HSDT effects, ( $I_1, \dots, I_9, I_{xx}^p, I_{yy}^p, I_{\phi\phi}^p, b_1, \tilde{I}_p$ ) are structural and mass quantities, ( $\tilde{a}_{Pi}, a_{Pi}$ ) are global piezoelectric coefficients, and  $R[z]$  contains the centrifugal stiffening effect (details omitted).

The surface charge density on actuators due to applied voltage is given by

$$\bar{\sigma}[z;t] = \boldsymbol{\Phi}_7^T[z] \hat{\mathbf{g}}[t] \quad (10)$$

where  $\hat{\mathbf{g}}[t]$  is the control input to be determined via LQR control. The displacement field is expressed in terms of trial functions and generalized coordinates as

$$u_o = v_o = w_o = \theta_x = \theta_y = \phi = \psi_o = (\boldsymbol{\Phi}_1^T[z] \mathbf{q}_1[t], \dots, \boldsymbol{\Phi}_7^T[z] \mathbf{q}_7[t]) \quad (11)$$

Using the extended Galerkin method (Shete et al. [5]) and eliminating the electrical degree of freedom  $\psi_o$  via Eq.(8), the discretized system resulting from the displacement governing equations is obtained as

$$\mathbf{M}\ddot{\mathbf{q}} + \mathbf{G}\dot{\mathbf{q}} + \mathbf{K}\mathbf{q} = \mathbf{Q}[t] - \mathbf{F}\hat{\mathbf{g}}[t]; \quad \mathbf{q} = \{\mathbf{q}_1^T | \dots | \mathbf{q}_6^T\}^T \quad (12)$$

The quantities  $\mathbf{G}|_{6N \times 6N}$ ,  $\mathbf{Q}|_{6N \times 1}$ ,  $\mathbf{F}|_{6N \times N}$ , and  $\hat{\mathbf{g}}|_{N \times 1}$  represent the gyroscopic matrix due to rotor, external forcing, piezoelectrically induced forcing coefficients, and time dependent charge density vector applied on actuators, respectively.

### 3. OPTIMAL CONTROL

#### 3.1 Sensor Output

Applying Gauss' law on the exposed surface of sensors, the total charge generated is given as

$$\tilde{q}_p = \int_z \oint_s D_3 S_s f_z ds dz |_{n=h/2} \quad (13)$$

Since no voltage is applied to sensors and  $\varepsilon_{ss} = 0$ , the  $n$ -component of electric displacement is  $D_3 = \zeta_{31} \varepsilon_{zz}$ . Introducing the strain  $\varepsilon_{zz} (= w')$  and performing the spatial discretization yields

$$\tilde{q}_p[t] = \mathbf{Cq}; \quad \mathbf{C} = [\mathbf{C}_1 | \cdots | \mathbf{C}_6] \quad (14)$$

with  $\mathbf{C}_i, i = 1, \dots, 6$ , being  $N$ -dimensional row vectors (details omitted). The sensor patches are treated as capacitors with capacitance  $C_p = \xi_{33} A_p / t_p$ , where  $A_p$  is the patch surface area. Hence, the voltage applied on actuators is given as

$$u[t] = 1/C_p \int_0^L \int_0^{2\kappa} \boldsymbol{\varphi}_7^T \hat{\mathbf{g}}[t] A_s f_z ds dz \quad (15)$$

Here  $S_s, A_s$  denote  $s$ -wise distribution of sensors and actuators, respectively, and  $f_z$  is their spanwise distribution. The current from sensors is  $I[t] = \tilde{q}_p$  and power required is  $P = uI$ .

#### 3.2 LQR Control

Using  $\mathbf{x} = \{\mathbf{q}^T | \dot{\mathbf{q}}^T\}^T$ , the state space representation of the system, i.e., Eq. (12), is

$$\dot{\mathbf{x}} = \mathbf{A}\mathbf{x} + \mathbf{B}\mathbf{Q} + \mathbf{W}\hat{\mathbf{g}}; \quad \mathbf{A} = \begin{bmatrix} \mathbf{0} & \mathbf{I} \\ -\mathbf{M}^{-1}\mathbf{K} & \mathbf{0} \end{bmatrix}; \quad \mathbf{B} = \begin{bmatrix} \mathbf{0} \\ \mathbf{M}^{-1} \end{bmatrix}; \quad \mathbf{W} = \begin{bmatrix} \mathbf{0} \\ -\mathbf{M}^{-1}\mathbf{F} \end{bmatrix} \quad (16)$$

One seeks the optimal control input  $\hat{\mathbf{g}}[t]$  that minimizes the cost index

$$J_a = \int_{t_0}^{t_f} (\mathbf{x}^T \mathbf{Z} \mathbf{x} + \hat{\mathbf{g}}^T \mathbf{R} \hat{\mathbf{g}}) dt \quad (17)$$

where  $\mathbf{R}$  is the positive definite control weighting matrix chosen as  $\mathbf{R} = \eta \mathbf{F}^T \mathbf{K}^{-1} \mathbf{F}$ ,  $\mathbf{Z}$  is the positive semi-definite state weighting matrix representing mechanical energy, i.e.,  $\mathbf{Z} \mathbf{x} = [\alpha \mathbf{q}^T \mathbf{K}^T | \mu \dot{\mathbf{q}}^T \mathbf{M}^T]^T$ , and  $\alpha, \mu, \eta$  are suitably chosen weights. The cost minimization yields the optimal control input as

$$\hat{\mathbf{g}} = -\mathbf{G}\mathbf{x}; \quad \mathbf{G} = \mathbf{R}^{-1} \mathbf{W}^T \mathbf{P} \quad (18)$$

where  $\mathbf{P}$  is the solution of the Algebraic Riccati Equation (ARE)

$$\mathbf{A}^T \mathbf{P} + \mathbf{P} \mathbf{A} - \mathbf{P} \mathbf{W} \mathbf{R}^{-1} \mathbf{W}^T \mathbf{P} + \mathbf{Z} = \mathbf{0} \quad (19)$$

The ARE is solved using stable eigenvectors of the Hamiltonian matrix of the LQR system (Potter [14]). Hence, from Eqs. (15) and (18), the actuator voltage for optimal control is given by

$$u[t] = -\hat{\mathbf{G}}\mathbf{x}; \quad \hat{\mathbf{G}} = 1/C_p \int_0^L \int_0^{2\kappa} \boldsymbol{\varphi}_7^T \mathbf{R}^{-1} \mathbf{W}^T \mathbf{P} \mathbf{A}_s f_z ds dz \quad (20)$$

In order to avoid saturation of the piezoactuators the voltage is limited to  $\text{sgn}[u]V_{\max}$  whenever  $|u| \geq V_{\max}$ , where  $V_{\max}$  is the actuator saturation voltage.

#### 4. RESULTS AND DISCUSSIONS

A single ply Graphite-Epoxy host structure is considered. The properties for the host and piezopatches (PZT-4) are taken from Song et al. [3]. The data used is  $R_0 = 0.2032$  m,  $L = 2.032$  m,  $b = 0.0254$  m,  $c = 0.127$  m,  $h = 0.0127$  m,  $\kappa = 0.0381$  m,  $t_p = 0.00127$  m, taper ratio  $\sigma = c_{\text{tip}}/c_{\text{root}} = 0.25$ ,  $m_R = m = 1$  kg. The trial functions satisfying BC's at the root are  $\boldsymbol{\varphi}_1 = \boldsymbol{\varphi}_2 = \boldsymbol{\varphi}_6 = \{z^2 z^3 z^4 \dots\}^T$ ,  $\boldsymbol{\varphi}_3 = \boldsymbol{\varphi}_4 = \boldsymbol{\varphi}_5 = \boldsymbol{\varphi}_7 = \{z z^2 z^3 \dots\}^T$ . The default case is for HSDT and a linearly pretwisted beam, with  $\Omega = 100$  rad/s,  $p_m = 875.63$  Nm<sup>-1</sup>, and piezopatch pair extending over the span. The nondimensional controlled tip response  $v_o^* = v_o[L;t]/L$ , control voltage  $u$ , and power  $P$  are plotted.

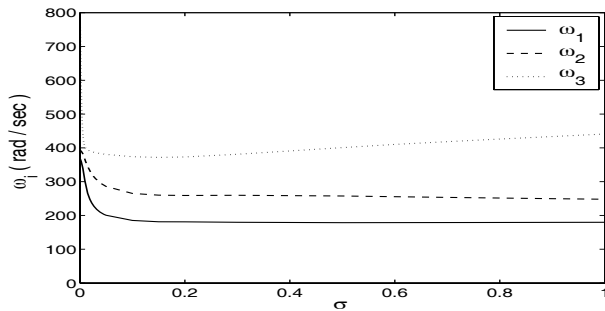


Figure 3. Effect of taper on eigenfrequencies.

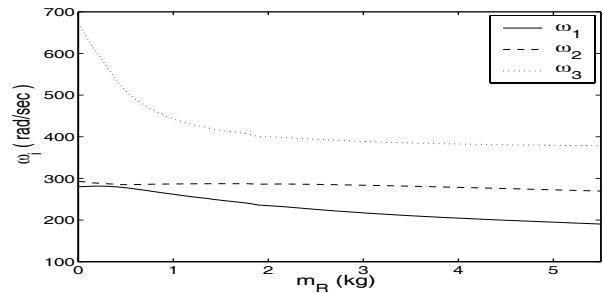


Figure 4. Effect of tip mass on eigenfrequencies.

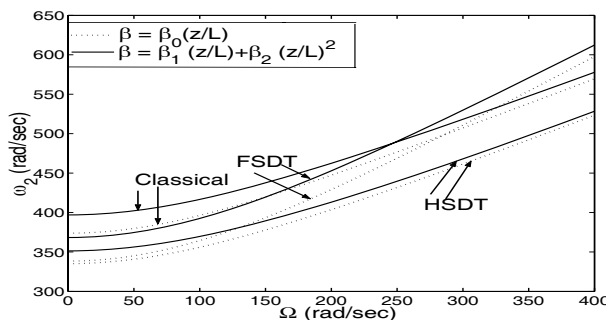


Figure 5. Comparison of three theories.

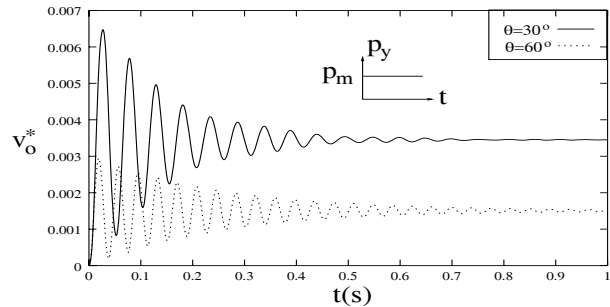


Figure 6. Response for uniform electric field [5].

Figure 3 shows the effect of taper on the eigenfrequencies for pretwist  $\beta_0 = 15^\circ$ , ply-angle  $\theta = 45^\circ$ , beam speed  $\Omega = 200$  rad/s, and rotor speed  $\bar{\Omega} = 200$  rad/s. There is a rapid decrease in the eigenfrequencies in the range  $0 \leq \sigma \leq 0.05$ . For  $\sigma \geq 0.2$  the taper has a negligible effect on the first two frequencies, and the third one shows a stiffening effect when the taper is reduced. The gyroscopic softening effect appears in Fig. 4 where the rotor mass causes a reduction in eigenfrequencies (especially the first and third ones). Figure 5 show the comparison of the three formulations for linear and quadratically varying pretwist with  $\theta = 90^\circ$ ,  $\beta_1 = 45^\circ$ ,  $\beta_2 = 45^\circ$ ,  $\beta_0 = 90^\circ$ ,  $\bar{\Omega} = 250$  rad/s. The HSDT formulation yields the lowest coupled natural frequencies, thus providing conservative data for use in attaining non-

resonant passive as well as active control designs. This emphasizes the importance of considering variations in transverse shear across the beam wall.

A comparison of the present control scheme (i.e., electric field varying along span) with the one considered in Shete et al. [5] (i.e., uniform electric field) is done for the rotorless beam with  $\beta_0 = 30^\circ$ . The present scheme yields an order-of-magnitude reduction in settling time, control voltage, and power required, as well as lower response, as evident from Figs. 8-9 when compared to Figs. 6-7. When considering a saturation constraint on the actuator voltage, the peak power requirement is reduced fivefold as seen in Fig. 10. Gyroscopic forces due to the the tip rotor appear to have a pronounced qualitative effect on the response when considering structural tailoring along with active control. In contrast with the rotorless system (Fig. 8), when the tip rotor is present the response attenuation is greater for a smaller ply-angle beam (Fig. 11).

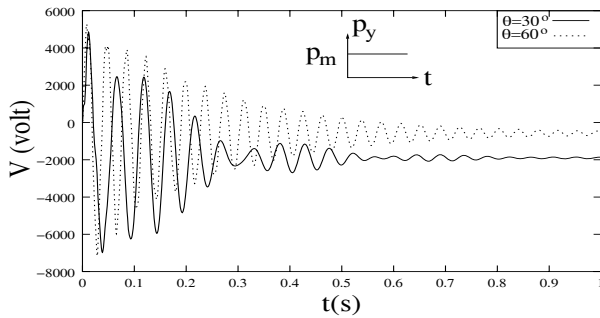


Figure 7. Voltage for uniform electric field [5].

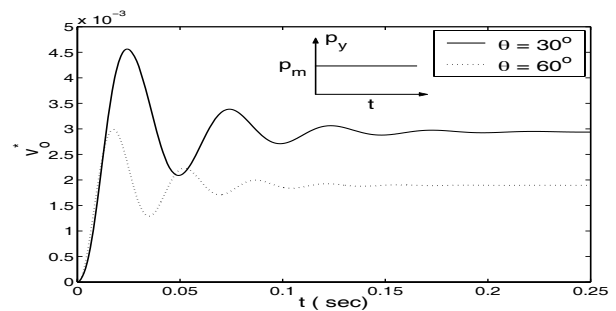


Figure 8. Response for nonuniform electric field.

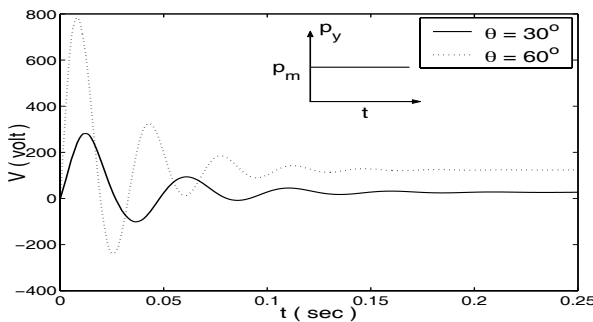


Figure 9. Voltage for nonuniform electric field.

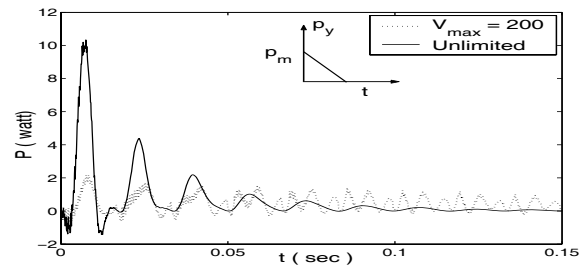


Figure 10. Effect of voltage constraint on power required.

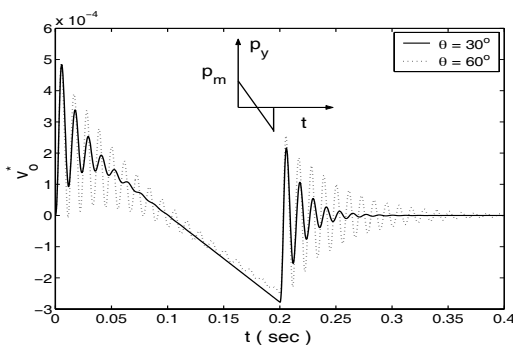


Figure 11. Response due to sonic boom.

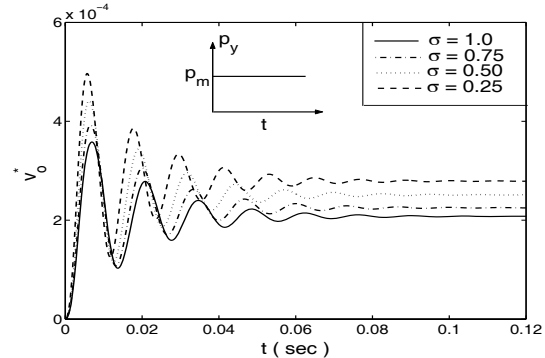


Figure 12. Effect of taper ratio on response.

Figure 12 shows the effect of taper on tip response, for  $\beta_0 = 30^\circ$ ,  $\theta = 30^\circ$ ,  $\Omega = 400 \text{ rad/s}$ ,  $\bar{\Omega} = 40 \text{ rad/s}$ , and step forcing. As expected, the response increases with taper, i.e., a uniform cross-section beam has the lowest response, due to its bending rigidity being uniformly higher over the span. Due to centrifugal stiffening arising from increased rotor mass, the response gets attenuated as shown in Fig. 13. When comparing the untwisted, linearly pretwisted, and parabolically pretwisted beam, the response is intermediate for

parabolic pretwist and lowest for linear pretwist as shown in Fig. 14. However, the control voltage and power is approximately the same for linear and parabolic pretwist.

## 5. CONCLUSIONS

A HSDT structural model for a rotating, doubly-tapered, pretwisted, composite blade, with piezoelectric sensors-actuator pairs, and a tip rotor is developed. The optimal control problem is studied for wide range of excitations. A spanwise varying electric field is considered, yielding a coupled electromechanical system as opposed to when a uniform field is considered. This results in increased attenuation, and reduced settling time and control voltage/power. The parametric studies performed underscore the importance of synthesizing active control and structural tailoring in achieving control effective designs.

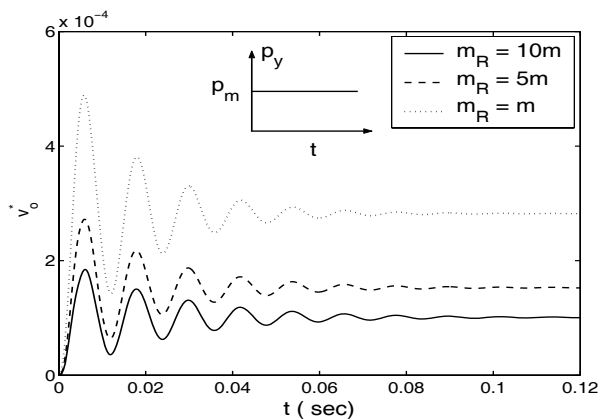


Figure 13. Effect of tip mass on response.

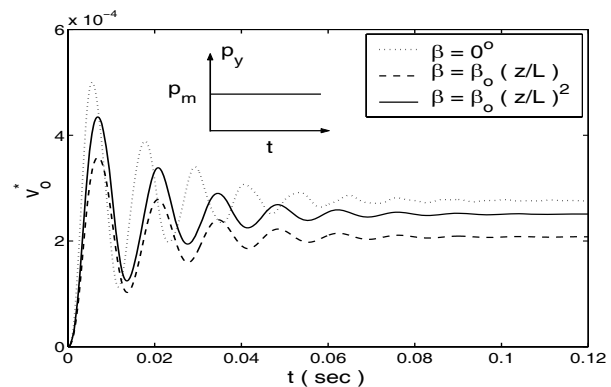


Figure 14. Effect of pretwist on response.

## REFERENCES

- [1] C. Kim and S. R. White, "Thick-walled composite beam theory including 3-D elastic effects and torsional warping", *International Journal of Solids and Structures* **34**(31-32), 4237-4259 (1997).
- [2] S. N. Jung, V. T. Nagaraj and I. Chopra, "Refined structural dynamics model for composite rotor blades", *AIAA Journal* **39**(2), 339-348 (2001).
- [3] O. Song, H. D. Kwon and L. Librescu, "Modeling, vibration, and stability of elastically tailored composite thin-walled beams carrying a spinning tip rotor", *J. Acoustical Society of America* **110**(2), 887-886 (2001).
- [4] N. K. Chandiramani, C. D. Shete and L. I. Librescu, "Vibration of higher-order-shearable pretwisted rotating composite blades", *International Journal of Mechanical Sciences* **45**, 2017-2041 (2003).
- [5] C. D. Shete, N. K. Chandiramani and L. I. Librescu, "Optimal control of a pretwisted shearable smart composite rotating beam", *Acta Mechanica* (in press)(2007).
- [6] H. H. Yoo, J. Y. Kwak and J. Chung, "Vibration analysis of rotating pre-twisted blades with a concentrated mass", *Journal of Sound and Vibration* **240**(5), 891-908 (2001).
- [7] D. L. Kunz, "Multimode control of a rotating uniform cantilever beam", *Journal of Guidance, Control, and Dynamics* **25**(2), 193-199 (2002).
- [8] G. P. Cai and C. W. Lim, "Active control of a flexible hub-beam system using optimal tracking control method", *International Journal of Mechanical Sciences* **48**, 1150-1162 (2006).
- [9] K. Wei, G. Meng, S. Zhou and J. Liu, "Vibration control of variable speed/acceleration rotating beams using smart materials", *Journal of Sound and Vibration* **298**, 1150-1158 (2006).
- [10] S. C. Choi, J. S. Park and J. H. Kim, "Vibration control of pretwisted rotating composite thin-walled beams with piezoelectric fiber composites", *Journal of Sound and Vibration* **300**, 176-196 (2007).
- [11] M. C. Ray, "Optimal control of laminated plate with piezoelectric sensor and actuator layers", *AIAA Journal* **36**(12), 2204-2208 (1998).
- [12] J. H. Han and I. Lee, "Optimal placement of piezoelectric sensors and actuators for vibration control of a

- composite plate using genetic algorithms”, *Smart Materials and Structures* **8**, 257-267 (1999).
- [13] W. Liu, Z. Hou and M. A. Demetriou, “A computational scheme for the optimal sensor/actuator placement of flexible structures using spatial  $H^2$  measures”, *Mechanical Systems and Signal Processing* **20**, 881-895 (2006).
- [14] J. E. Potter, “Matrix Quadratic Solutions”, *SIAM Journal of Applied Mathematics* **14**(3), 496-501 (1966).